Bandwidth enhancement of inter-modal four wave mixing Bragg scattering by means of dispersion engineering

Omar F. Anjum,[1] Peter Horak,[1] Yongmin Jung,[1] Masato Suzuki,[2] Yoshinori Yamamoto,[2] Takemi Hasegawa,[2] Periklis Petropoulos,[1] David J. Richardson,[1] and Francesca Parmigiani[1, a)]

[1)] *Optoelectronics Research Centre, University of Southampton, Southampton SO17 1BJ, UK*

[2)] *Optical Communications Laboratory, Sumitomo Electric Industries, Ltd., Yokohama 244-8588, Japan*

(Dated: 9 October 2018)

We report on the design, fabrication and experimental characterization of Germanium-doped graded-index multi-mode fibers that are tailored to achieve broadband operation for the inter-modal Bragg scattering four wave mixing process. Firstly, we show that increasing the core diameter decreases the separation between the pumps and the signal/idler pair. Secondly, we demonstrate a conversion efficiency bandwidth (7 nm) of more than twice that achieved previously with half the fiber length (50 m).

PACS numbers: Valid PACS appear here
Keywords: Higher order mode, Fiber nonlinear optics, Optical wavelength conversion, Four-wave mixing, Optical signal processing

I. INTRODUCTION

Four-wave mixing (FWM), the parametric interaction of electromagnetic waves mediated by the $\chi^{(3)}$ susceptibility, has a broad range of applications in the field of optical communications. For a given configuration of input frequencies, FWM processes typically result in the creation of fields at new frequencies, commonly referred to as idlers. The ultrafast nonlinear response time of the $\chi^{(3)}$ nonlinearity allows the idler to follow any rapid phase or amplitude variations of an input signal, making it transparent to the signal modulation format. For this reason, FWM has attracted attention as a means to implement a variety of all-optical signal processing functionalities[1–4]. Among the various implementations of FWM, the Bragg Scattering (BS) process has been proposed as an efficient and ideally noiseless mechanism for wavelength conversion[5], with important applications in both classical lightwave systems as well as quantum communication[6,7].

The configuration of interacting waves shown in Fig. 1 highlights some key features of the BS process. Inputs $p1$ and $p2$ at frequencies ω_{p1} and ω_{p2} respectively are high intensity applied fields (referred to as the pumps). In typical fiber optic implementations, their frequency separation (given by $\Delta\omega_{pp} = \omega_{p1} - \omega_{p2}$) is of the order of several hundreds of GHz. The input signal s at ω_s is separated from the pumps by $\Delta\omega_{ps} = \omega_s - \omega_{p2}$ (note that below we will occasionally refer to $\Delta\lambda$ as the wavelength separation corresponding to $\Delta\omega$). The energy conservation relation to generate the

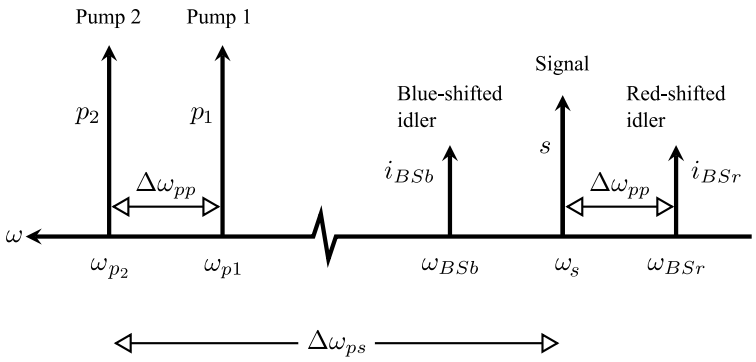

FIG. 1. Frequency allocation in a FWM BS process.

[a)] Now with Microsoft Research, Cambridge, CB1 2FB, U.K.

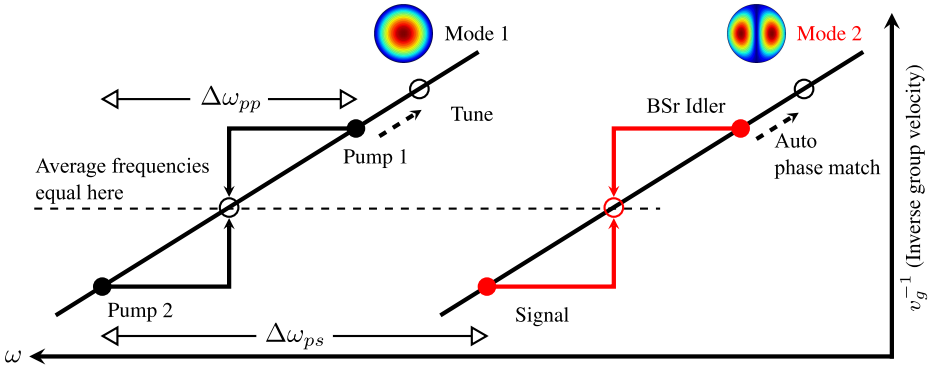

FIG. 2. Illustration of the relationship between the inverse group velocity (IGV) curves of the participating modes. The IGV curves need to be parallel in order to satisfy phase matching for the BSr idler when pump 1 is tuned.

red-shifted idler i_{BSr} at ω_{BSr} is given by $\omega_{BSr} + \omega_{p2} \rightarrow \omega_s + \omega_{p1}$, implying the creation of $p2$ and i_{BSr} photons and the annihilation of s and $p1$ photons. A similar relation holds for the blue-shifted idler, i_{BSb}, at ω_{BSb}. The idler frequencies are shifted from that of the signal by $\Delta\omega_{pp}$. FWM idlers require phase matching for efficient generation. In single-mode fibers and waveguides phase matching is typically realized by utilizing a scheme that places the pump and signal wave frequencies symmetrically around the zero dispersion wavelength (ZDW)[8] of the fiber. Developments in space division multiplexing, advanced fiber fabrication, and the ability to independently launch and control high order modes (HOMs) have also motivated recent interest in nonlinear effects in multimode fibers (MMFs)[9–13]. In this context, processes such as FWM offer the possibility to simultaneously access spatial and spectral degrees of freedom of light propagation, thus allowing for a multitude of novel ultra-fast signal processing applications.

The phase matching conditions for the observation of inter-modal FWM BS are quite distinct relative to the single-mode case. Referring again to Fig. 1, the pair of pumps in an inter-modal BS system excite one propagation mode (e.g. LP_{01}) while the signal excites a different one (e.g. LP_{11}). Then, the generated idler at ω_{BSr} in the LP_{11} mode is phase-matched if the inverse group velocity (IGV) curves evaluated at the average frequency of the waves in the same mode are nearly equal for the two modes (see Fig. 2)[10,11]. In other words, for a small frequency detuning ($\Delta\omega_{pp} \approx 0$), phase matching is achieved if a horizontal line can be drawn in Fig. 2 to intersect both IGV curves at the values corresponding to the mean frequencies of the waves in each mode. Furthermore, broadband phase matching (i.e. phase-matching for large detuning $\Delta\omega_{pp}$) for the BSr idler is achieved when the IGV curves of the two modes are horizontally shifted replicas of one another[14]. However, the same phase-matching property cannot hold simultaneously for both the BSr and the BSb idlers. Phase-matching of only a specific nonlinear process, i.e. the generation of the BSr idler but not of the BSb idler, is a helpful feature in optical processors for wavelength division multiplexed (WDM) systems, since the onset of any undesired idler represents a leakage of pump energy and will degrade the overall system performance by inducing inter-modal cross-talk with neighboring frequency channels.

By engineering the IGV curves and their relative frequency separation $\Delta\omega_{ps}$, the signal can be placed far away from the pumps, thereby preventing contamination by undesired amplified spontaneous emission (ASE) noise associated with high pump powers or by Raman effects. Moreover, since efficient idler generation does not require low or anomalous dispersion values, suppression of undesired intra-modal FWM idlers can also be achieved by properly optimizing the fiber dispersion profiles of the various modes.

Inter-modal FWM BS processes have recently been demonstrated both in fibers[15] and in silicon waveguides[16]. Specifically, we have theoretically and experimentally studied phase-matching, uni-directionality of conversion and insensitivity to pump polarization in IM FWM processes in randomly birefringent fibers guiding a small number of modes[11,14,15]. In Ref. 15, we focused on the IM FWM BS process in an elliptical core three-mode graded-index fiber, achieving phase matching for only the BSr idler with $\Delta\lambda_{ps}$ of about 25 nm (40 nm) for the LP_{01}-LP_{11a} (LP_{01}-LP_{11b}) pump-signal mode groups. Using 50 m of that fibre we demonstrated $\Delta\lambda_{pp}$ bandwidths of up to 3 nm[15]. In this paper, we report on the design, fabrication and characterization of several 100 m long graded-index (GI) MMFs to specifically demonstrate the bandwidth enhancement for the IM FWM BS process through dispersion engineering, reporting $\Delta\lambda_{pp}$ bandwidths of up to 7 nm. This length was chosen to provide balance between idler gain and CE bandwidth, given that bandwidth decreases with length whereas gain increases. Some of the preliminary results of this work have been reported in Ref. 17.

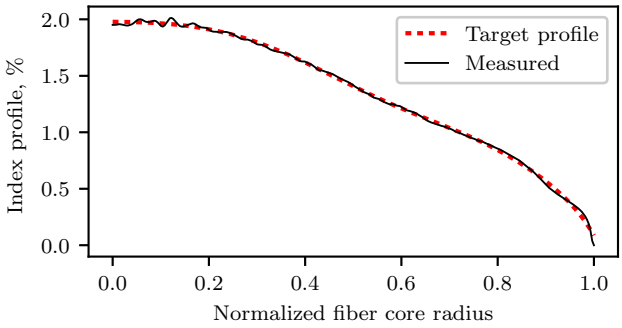

FIG. 3. Refractive index of the fabricated GI MMF core (solid line) and the profile used for numerical optimization of the fiber design (dashed line).

II. FIBRE DESIGN, FABRICATION AND CHARACTERIZATION

A set of dispersion-tailored optical fibers was designed and fabricated to achieve large $\Delta\omega_{pp}$ bandwidths for the phase-matched IM FWM BSr process as shown in Fig. 2, i.e. with two pump waves in the fundamental mode (LP_{01}) and signal and generated idlers in the first higher order mode (LP_{11}). All fibers under test (FUTs) are based on the same GI fiber core made of highly GeO_2-doped SiO_2 having a quasi-parabolic index profile (see Fig. 3). The core has a peak index difference of 2.0% relative to the cladding and a fitted alpha-power of 2.1 in the range of radii up to 50% of the core radius where our modes of interest are confined. The core was surrounded by a pure SiO_2 cladding and drawn to several fibers of length 100 m and with four core diameters ranging from 18.1 μm to 25.3 μm.

First, we experimentally measured the IGV curves of the supported modes of all GI MMFs using a time-of-flight (TOF) method[18]. IGV curves of the modes of interest, namely LP_{01} and LP_{11}, are shown for the 24.1 μm and 25.3 μm core diameter fibers in Fig. 4(a) and (b), respectively. From these, horizontal separations of about 33 nm and 23 nm between the two IGV curves can be estimated. These values correspond to the wavelength spacings $\Delta\lambda_{ps}$ necessary to achieve phase matching between the two modes (as will be verified later in this article). The slope of an IGV curve evaluated at a particular wavelength gives the dispersion parameter at that wavelength. Using a linear fit to the measured IGV curves, we estimate chromatic dispersion values of 14.2 ps/nm/km (12.5 ps/nm/km) for the LP_{01} mode and 13.6 ps/nm/km (11.4 ps/nm/km) for the LP_{11} modes for the 24.1 μm (25.3 μm) diameter core fibers. Clearly, a large difference in the dispersion parameters between modes will lead to small $\Delta\lambda_{pp}$ bandwidths (see Fig. 2). Fig. 4(c) shows experimentally measured relative IGVs for all measurable modes of the 25.3 μm fiber. Effective areas for the 25.3 μm fiber were calculated to be 55.7 μm^2 (LP_{01}) and 75.6 μm^2 (LP_{11}). For the 24.1 μm fiber, the areas were 52.8 μm^2 (LP_{01}) and 72.4 μm^2 (LP_{11}).

Based on our TOF analysis, the total number of modes supported by the fibers is greater than ten. In principle, different mode pairs among these can be used to achieve phase-matching in frequency bands further apart than in the LP_{01}-LP_{11} mode pair. Note that mode characterization using the TOF method is limited by several factors including photodetector bandwidth, the length of the fibers, and the initial temporal pulse width of the optical source that was available for our experiments. Our characterization was done using a mode-locked fiber laser producing 0.5 ps pulses with a repetition rate of 20 MHz and 4 mW of average power. Each pulse undergoes dispersion inside the FMF, and the delays of the resulting modal components are measured on a 10 GHz oscilloscope. Based on these parameters, we could not precisely quantify IGV behavior at points where the modal delays became too small (of the order of 50 ps over 100 m) which results in the only partially completed IGV curves in Fig. 4(c).

The separation $\Delta\lambda_{ps}$ between the IGV curves of the LP_{01} and LP_{11} modes for all four fibers is shown in Fig. 5. Note that a linear fit was used in order to extrapolate the IGV curves beyond the measured wavelength range. Our simulations based on the refractive index profile of Fig. 3 predict the same trend as the measurements: an increase in core diameter of the GI MMF corresponds to a reduction of $\Delta\lambda_{ps}$. Note that in the results presented in Fig. 5, we used the material dispersion of pure silica in our simulations, which is larger than that of the germanium-doped core material and thus over-estimates the slope of the IGV curves.

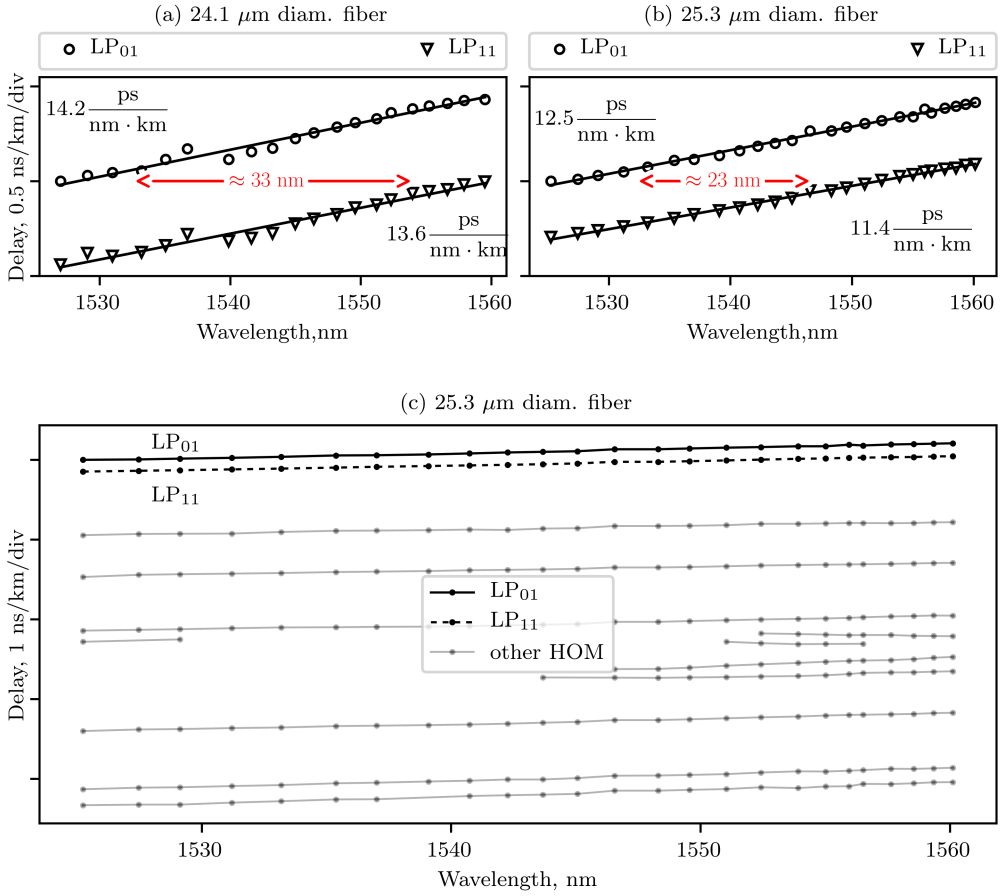

FIG. 4. (a) and (b) Relative IGV curves for the modes of interest (LP_{01} and LP_{11}) for the two fibers (24.1 μm and 25.3 μm diameter cores, respectively). (c) Relative IGVs of all the modes of the 25.3 μm diameter fiber. All the curves were measured using the TOF method.

III. EXPERIMENTAL SET-UP

The experimental set-up for IM FWM is shown in Fig. 6. Three continuous-wave (CW) laser sources were used to produce the applied optical beams (two pumps and a signal) at the fiber input. The pumps were launched into the fundamental mode. The signal wave was launched into the LP_{11} mode using a free-space phase-plate (PP) that provided a π phase shift across the center of the CW source beam. The inputs in the two modes were coupled using a free-space beam-splitter and their polarizations were aligned at the fiber input by a combination of polarization controllers and a (free-space) polarizing beam-splitter (PBS). A two-mode fiber (TMF), which makes it easier to selectively launch the LP_{11} mode for coupling into the FMF, was spliced to the input of our GI MMF to increase the modal purity inside the fiber.

At the GI MMF output, the different spatial modes were extracted using a free-space mode-demultiplexer (MDMUX) based on the same principle as the MMUX. Here, the PPs reverse the phase-changes associated with HOMs, making it possible for light in a HOM to be coupled efficiently into a single-mode fiber. Note that even though the MMUX excites only one of the degenerate LP_{11} modes, linear mode mixing occurs during propagation in the GI MMF between the LP_{11a} and LP_{11b} modes and thus two orthogonally orientated PPs in the MDMUX are essential in order to fully measure the output power in the LP_{11} mode group. An optical switch enables the selection and independent measurement of each of the MDMUX output ports on an optical spectrum analyser (OSA). Both the MMUX and MDMUX give mode extinction ratios of up to 20 dB.

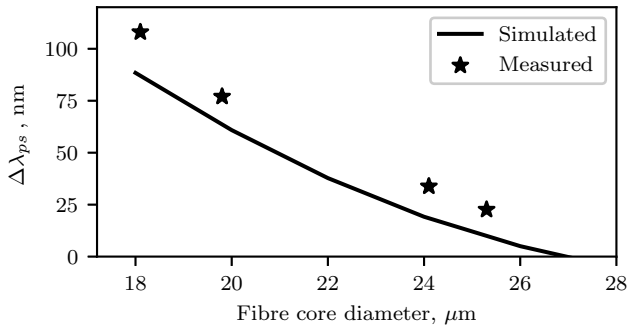

FIG. 5. Simulated (line) and measured (stars) pump-to-signal wavelength detuning, $\Delta\lambda_{ps}$, as a function of the core diameter of the GI MMF.

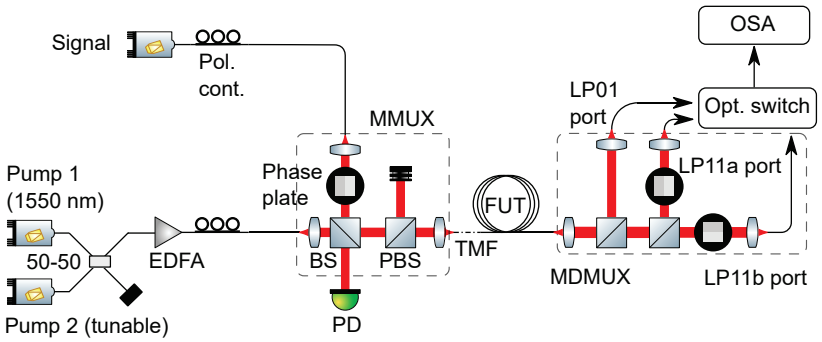

FIG. 6. Inter-modal FWM experimental set-up.

IV. NUMERICAL AND EXPERIMENTAL RESULTS

Next, with the input wave configuration shown in Fig. 1, we simulated the conversion efficiency (CE) of the BSr and BSb idlers versus $\Delta\lambda_{pp}$ for the 25.3 μm and 24.1 μm diameter fibers. We define the CE as the ratio of output idler power to output signal power as this is easily accessible experimentally and only a small fraction of power is converted from the signal. The total pump power into the fiber was about 23.5 dBm, while the signal power was about 8.5 dBm. While these input powers may induce Stimulated Brillouin Scattering (SBS) in typical single mode fibers, in our experiments we did not experience SBS due to the FMFs having higher effective areas and relatively short lengths. The wavelength of $p2$ was fixed at 1550 nm while that of $p1$ was varied. The signal wavelength (and therefore $\Delta\omega_{ps}$) was determined in accordance with the measurements summarized in Fig. 5. The simulation results were obtained by solving the multi-mode generalized nonlinear Schrödinger equation[19] using the measured IGV with linear fitting.

Simulated CE curves against $\Delta\lambda_{pp}$ for the two fibers are shown in Fig. 7 for two different values of $\Delta\lambda_{ps}$. Fig. 7(a) and (c) correspond to the CE at the theoretical phase matching points specified in Fig. 5 for the respective core diameters, whereas (b) and (d) correspond to $\Delta\lambda_{ps}$ values that yield the maximum -3 dB bandwidth obtainable. For both fibers it was found that by tuning the signal wavelength away from the theoretical phase matching point by less than 0.6 nm, it is possible to enlarge the overall bandwidth by allowing for a small reduction in CE in the middle of the band. The maximum BSr CE bandwidth for the 25.3 μm (24.1 μm) fiber is about 9 nm (10 nm) at the theoretical phase matching point, which increases to a maximum of 18 nm (24 nm) by optimizing $\Delta\lambda_{ps}$. On the other hand, for the BSb idler the -3 dB bandwidths are of the order of 0.5 nm in all cases. The absolute CE is about -32 dB. We note that the periodic oscillations in the CE are due to the power oscillating between signal and idler along the fiber length if the phase matching condition is not fulfilled.

Subsequently, we carried out the corresponding experiments. First, we verified that the estimated values of $\Delta\lambda_{ps}$ in Fig. 5 lead to efficient BSr idler generation. This was done by keeping the wavelengths of $p1$ and $p2$ constant at 1552.5 nm and 1550 nm, respectively, while scanning the signal wavelength around its predicted value. The BSr (normalized) CE as a function of signal wavelength (or equivalently $\Delta\lambda_{ps}$) is plotted in Fig. 8 for both fibers. Idler generation was observed for a small range of signal wavelengths centered on 23 nm (35 nm) separation from pump $p1$

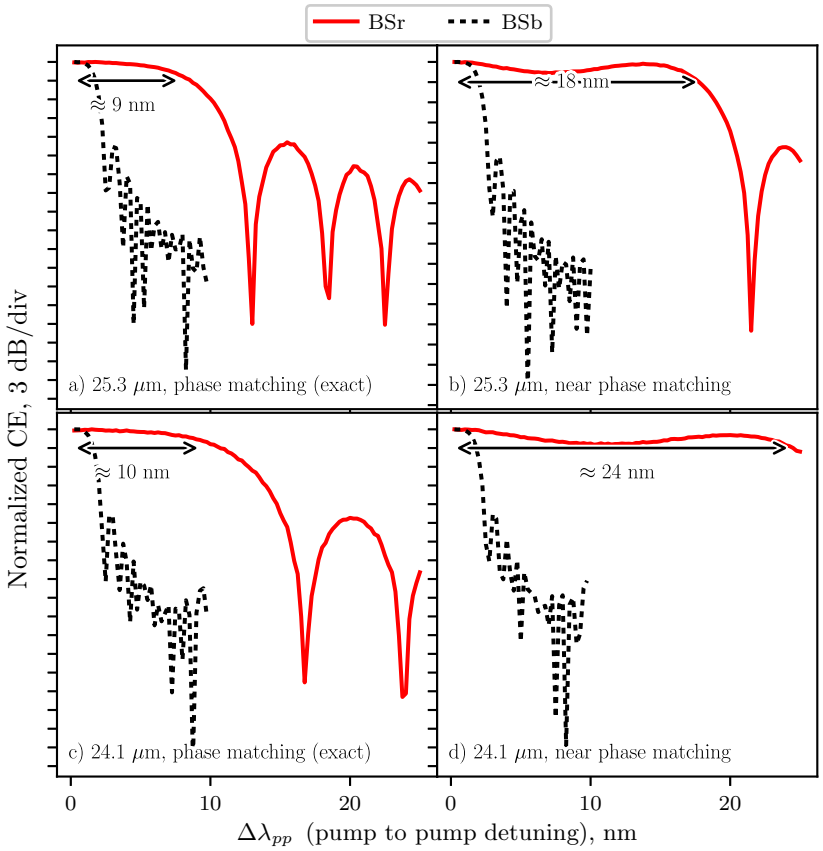

FIG. 7. Simulated normalized CE of the BSr and BSb processes with respect to pump to pump detuning $\Delta\lambda_{pp}$ for the 25 μm and 24.1 μm diameter GI MMFs. (a) and (c) CE for the signal wavelength corresponding to $\Delta\lambda_{ps}$ = 23 nm and 33 nm respectively. b) and d) Here, $\Delta\lambda_{ps}$ differs from the corresponding values in (a) and (c) by about 0.6 nm.

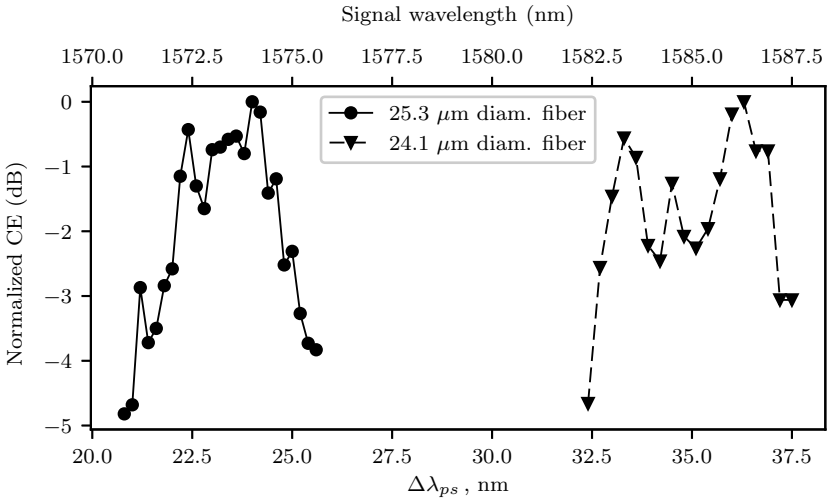

FIG. 8. The variation of CE with signal detuning $\Delta\lambda_{ps}$ (from fixed pumps) for the two fibers. Pump wavelengths are λ_{p1} = 1550 nm and λ_{p2} = 1552.5 nm.

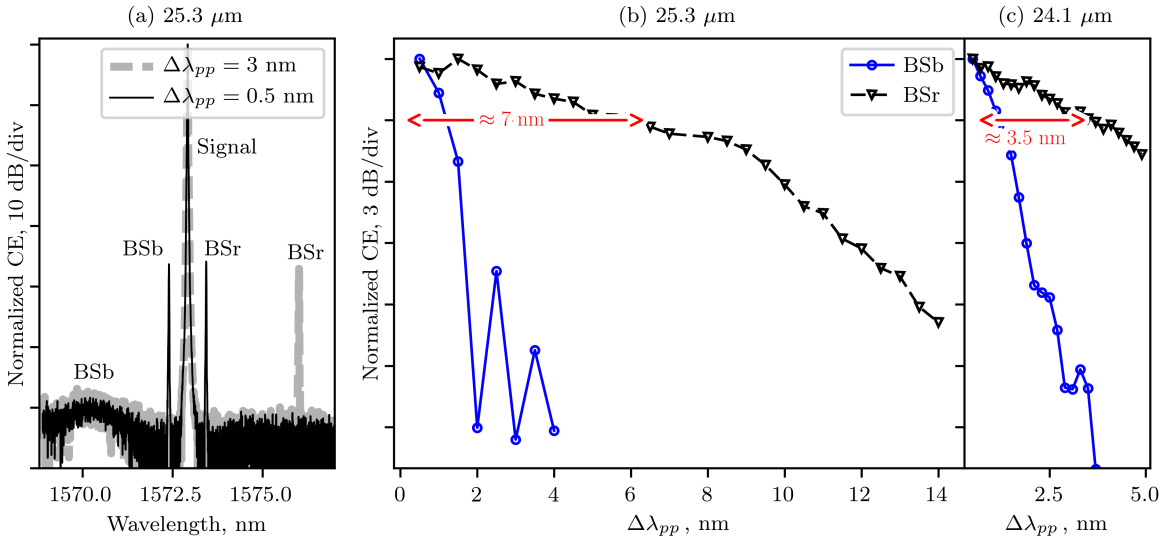

FIG. 9. a) Measured spectral traces for $\Delta\lambda_{pp}$ equal to 0.5 nm and 3 nm for the 25.3 μm fiber. b) and c) Normalized CEs of the BSb and BSr processes with respect to $\Delta\lambda_{pp}$ for the 25.3 μm and 24.1 μm core diameter GI MMFs.

for the 25.3 μm (24.1 μm) core diameter fiber, thus showing good agreement with the results presented in Fig. 5.

We then characterized the CE behavior of the BSb and BSr idlers as $\Delta\lambda_{pp}$ was varied. The signal wavelength was adjusted to achieve the broadest bandwidth. Fig. 9(a) shows typical IM FWM spectra obtained at the recombined LP_{11} MDMUX output port for two values of $\Delta\lambda_{pp}$ (0.5 nm and 3 nm) when using the 25.3 μm core diameter fiber (hence $\Delta\lambda_{ps} \approx 23$ nm). As predicted from the simulations, when $\Delta\lambda_{pp}$ increases from 0.5 nm to 3 nm the power of the phase matched BSr idler remains fairly constant, while the non-phase matched BSb idler vanishes for $\Delta\lambda_{pp} > 3$ nm. This provides more than 20 dB extinction between the desired (BSr) idler and the unwanted one (BSb). The optical signal to noise ratios of both BSr idlers are more than 20 dB, and the corresponding measured CEs are about -35 dB. The relatively low CE values are in part due to the large core diameters of the 100 m long fibers as well as the relatively low pump powers used, and could be improved significantly by implementing more complex fiber designs with smaller cores or by moving to materials with higher nonlinearity.

The normalized CE as a function of $\Delta\lambda_{pp}$ for the two fibers is shown in Fig. 9(b) and (c). For the 25.3 μm diameter fiber, a -3 dB half-bandwidth of about 7 nm (0.5 nm) was obtained for the BSr (BSb) idler. This result represents a bandwidth enhancement (for BSr) of more than 100% as compared to our previously reported work in a non-dispersion-engineered fiber with half the length of this fiber. This also highlights that it is possible to selectively phase match only the desired nonlinear process (BSr versus BSb) by properly engineering the spatial modes of the fiber. Note that this feature cannot be attained only by dispersion engineering a low-birefringence single mode fiber. This uni-directionality of FWM BS was also recently demonstrated by exploiting the polarization modes of a silicon waveguide[6]. For the 24.1 μm diameter fiber, the measured 3 dB half-bandwidth was reduced to 3.5 nm (0.5 nm) for the BSr (BSb) idler.

We attribute the discrepancy between the simulated and experimental bandwidths to be firstly due to higher order dispersion terms, which were not included in the simulations, because they could not be derived with confidence from the IGV measurements over a limited wavelength range. These play a more critical role in the FWM process as $\Delta\omega_{ps}$ increases, i.e. in the 24.1 μm diameter fiber. To better appreciate the implications of higher order dispersion in simulations, the wavelength range of the measured IGV curves would have to be enlarged, which is not currently possible in our lab. Secondly, FWM is affected by stochastic variations of key fiber parameters (e.g. core radius) along the fabricated fiber length which are inherent in the manufacturing process[11,20].

V. CONCLUSIONS

We have reported on the design, fabrication and characterization of graded index multi-mode fibers that were dispersion engineered to provide broadband operation for the phase matched inter-modal Bragg Scattering FWM process. We experimentally measured bandwidths of up to 7 nm in a 100 m fiber, which are broader than those

obtained in previously published work in a fiber half this length. Better than 20 dB extinction between the desired and undesired idler was measured, highlighting the capability to control the phase matching properties of specific FWM processes by exploiting the spatial fiber modes. The uni-directionality of the FWM process is a key factor in achieving highly efficient wavelength conversion and in efficient control of output wavelengths to avoid nonlinear cross-talk between adjacent wavelength division multiplexed channels.

ACKNOWLEDGMENTS

This research is sponsored by EPSRC grants EP/P026575/1 and EP/P030181/1. The data for this work are accessible through the University of Southampton Institutional Research Repository at https://doi.org/10.5258/SOTON/D0672.

[1]S. L. I. Olsson, B. Corcoran, C. Lundström, T. A. Eriksson, M. Karlsson, and P. A. Andrekson, "Phase-sensitive amplified transmission links for improved sensitivity and nonlinearity tolerance," J. Lightwave Technol. **33**, 710–721 (2015).

[2]R. Slavík, F. Parmigiani, J. Kakande, C. Lundström, M. Sjödin, P. A. Andrekson, R. Weerasuriya, S. Sygletos, A. D. Ellis, L. Grüner-Nielsen, D. Jakobsen, S. Herstrøm, R. Phelan, J. O'Gorman, A. Bogris, D. Syvridis, S. Dasgupta, P. Petropoulos, and D. J. Richardson, "All-optical phase and amplitude regenerator for next-generation telecommunications systems," Nature Photonics **4**, 690 EP – (2010).

[3]C. J. McKinstrie, S. Radic, and A. R. Chraplyvy, "Parametric amplifiers driven by two pump waves," IEEE Journal of Selected Topics in Quantum Electronics **8**, 538–547 (2002).

[4]T. Tanemura, C. S. Goh, K. Kikuchi, and S. Y. Set, "Highly efficient arbitrary wavelength conversion within entire c-band based on nondegenerate fiber four-wave mixing," IEEE Photonics Technology Letters **16**, 551–553 (2004).

[5]C. McKinstrie, J. Harvey, S. Radic, and M. Raymer, "Translation of quantum states by four-wave mixing in fibers," Optics Express **13**, 9131–9142 (2005).

[6]B. A. Bell, C. Xiong, D. Marpaung, C. J. McKinstrie, and B. J. Eggleton, "Uni-directional wavelength conversion in silicon using four-wave mixing driven by cross-polarized pumps," Opt. Lett. **42**, 1668–1671 (2017).

[7]H. J. McGuinness, M. G. Raymer, C. J. McKinstrie, and S. Radic, "Quantum frequency translation of single-photon states in a photonic crystal fiber," Phys. Rev. Lett. **105**, 093604 (2010).

[8]K. Uesaka, K. K. Y. Wong, M. E. Marhic, and L. G. Kazovsky, "Wavelength exchange in a highly nonlinear dispersion-shifted fiber: theory and experiments," IEEE Journal of Selected Topics in Quantum Electronics **8**, 560–568 (2002).

[9]J. Demas, P. Steinvurzel, B. Tai, L. Rishoj, Y. Chen, and S. Ramachandran, "Intermodal nonlinear mixing with bessel beams in optical fiber," Optica **2**, 14–17 (2015).

[10]R. J. Essiambre, M. A. Mestre, R. Ryf, A. H. Gnauck, R. W. Tkach, A. R. Chraplyvy, Y. Sun, X. Jiang, and R. Lingle, "Experimental investigation of inter-modal four-wave mixing in few-mode fibers," IEEE Photonics Technology Letters **25**, 539–542 (2013).

[11]S. M. M. Friis, I. Begleris, Y. Jung, K. Rottwitt, P. Petropoulos, D. J. Richardson, P. Horak, and F. Parmigiani, "Inter-modal four-wave mixing study in a two-mode fiber," Opt. Express **24**, 30338–30349 (2016).

[12]F. Poletti and P. Horak, "Dynamics of femtosecond supercontinuum generation in multimode fibers," Opt. Express **17**, 6134–6147 (2009).

[13]A. Bendahmane, K. Krupa, A. Tonello, D. Modotto, T. Sylvestre, V. Couderc, S. Wabnitz, and G. Millot, "Seeded intermodal four-wave mixing in a highly multimode fiber," J. Opt. Soc. Am. B **35**, 295–301 (2018).

[14]F. Parmigiani, P. Horak, Y. Jung, L. Grüner-Nielsen, T. Geisler, P. Petropoulos, and D. J. Richardson, "All-optical mode and wavelength converter based on parametric processes in a three-mode fiber," Opt. Express **25**, 33602–33609 (2017).

[15]O. F. Anjum, M. Guasoni, P. Horak, Y. Jung, P. Petropoulos, D. J. Richardson, and F. Parmigiani, "Polarization insensitive four wave mixing based wavelength conversion in few-mode optical fibers," Journal of Lightwave Technology , 1–1 (2018).

[16]C. Lacava, M. Ettabib, T. Bucio, G. Sharp, A. Khokhar, Y. Jung, D. Richardson, P. Petropoulos, F. Gardes, M. Sorel, and F. Parmigiani, "Inter-modal wavelength conversion in silicon waveguide," in *Proc. Eur. Conf. Opt. Comm., accepted* (2018).

[17]O. F. Anjum, P. Horak, Y. Jun, M. Suzuki, Y. Yamamoto, T. Hasegawa, P. Petropoulos, D. J. Richardson, and F. Parmigiani, "Broadband study of inter-modal bragg scattering four wave mixing in multi-mode fibres," in *Proc. Eur. Conf. Opt. Comm., accepted* (2018) p. We4E.4.

[18]J. Cheng, M. E. V. Pedersen, K. Wang, C. Xu, L. Grüner-Nielsen, and D. Jakobsen, "Time-domain multimode dispersion measurement in a higher-order-mode fiber," Opt. Lett. **37**, 347–349 (2012).

[19]F. Poletti and P. Horak, "Description of ultrashort pulse propagation in multimode optical fibers," J. Opt. Soc. Am. B **25**, 1645–1654 (2008).

[20]M. Guasoni, F. Parmigiani, P. Horak, J. Fatome, and D. J. Richardson, "Intermodal four-wave-mixing and parametric amplification in km-long multi-mode fibers," Journal of Lightwave Technology **PP**, 1–1 (2017).